

THERMOMECHANICAL MODELLING THE RESISTANCE WELDING OF PbSb ALLOY

by

**Dragan V. KALABA^a, Aleksandar S. SEDMAK^b,
Zoran J. RADAKOVIĆ^{b*}, and Marko V. MILOŠ^c**

^a Faculty of Mechanical Engineering at Kosovska Mitrovica,
University of Priština, Serbia

^b Faculty of Mechanical Engineering, University of Belgrade, Belgrade, Serbia

^c Faculty of Mechanical Engineering – Innovation Centre,
University of Belgrade, Belgrade, Serbia

Original scientific paper
UDC: 549.24/25:517.96:536.24
DOI: 10.2298/TSCI1002437K

The analytical modelling of the PbSb alloy resistance spot welding process has been developed on the basis of mathematical analysis of thermomechanical conservation laws. The numerical solution of partial differential equations, obtained by such modelling, has been achieved by the finite element method.

Thermomechanical equilibrium equations are derived, including specific properties, typical for PbSb alloys. The paper utilizes the basic experimentally proven assumption, that the temperature fields govern all processes during welding. Full agreement is evident between the experimental and analytical data.

Key words: mathematical modelling, resistance spot welding, PbSb alloy, finite elements, temperature field

Introduction

The complexity of the resistance spot welding process is represented by various parameters needed to describe the undergoing physical influences (*e. g.* electric current, electrical resistance, contact force, material type, temperature, *etc.*). By identifying the temperature field it becomes possible to simulate heating, deformation and cooling processes, and to ensure some basic assumptions for predicting structural changes at locations of the joint and its final mechanical properties.

Efforts for developing modern simulations of concern here have four orientations:

- implementing influences of latent heat and phase transformations in the numerical analysis [1-3],
- development of mathematical formulations of thermomechanical processes in resistance spot welding and their correlation to heat and electrical processes [4, 5],

* Corresponding author; e-mail: zradakovic@mas.bg.ac.rs

- quantification of the contact surface regardless of whether this surface is an electrode-to-sheet metal or sheet-to-sheet microcontact, as well as changes in geometry of the conductive media [4, 6], and
- implementing all particularities of the resistance spot welding of new materials and alloys into well established mathematical models.

Research on the problems of resistance welding of heavy alloys is relatively scarce and insignificant. Aside to theoretical research, of practical importance *i. e.* is the complicated assembly of lead-acid batteries. The resistance welding operation for the PbSb alloy grid cell joining is crucial, and the created residual stresses are the most frequent cause of failure in these welded joints.

The mathematical analysis of the heat process implicates mathematical modelling (finite elements) and defining the heat conduction equation. The process is further mathematically analysed and residual stresses are evaluated. Procedures are carried out for numerical integration of differential equations of heat conduction and residual stresses, with error estimation depending on the adopted finite element mesh.

Model formulation

Heat conduction equation

The welding process is represented by a thermomechanical model in the scope of basic laws of continuum mechanics. The global energy balance law in the coupled form [7-9] is

$$\int_{V_0} \rho_0 [(r \dot{u}) - T^{ij} v_{,j}^i] dV - \int_{A_0} h_0 dA_0 \quad (1)$$

where ρ_0 is the mass density, u – the strain energy density, r – the volume heat source, T^{ij} – the stress tensor, v^i – the velocity vector, h_0 – the surface heat flux, A_0 – the contour area, and V_0 – the volume encompassed by A_0 . The subscript “0” denotes undeformed (initial) configuration, “.” is the time derivative, and “,” – the partial derivative over Descartes co-ordinates x_j . Coupling of thermal and mechanical terms in eq. (1) is due to the following:

- second and fourth terms contain only thermal energy, the third contains only mechanical energy, and the first contains both,
- strain energy density depends on both temperature and strain, $U = u(t, e_{ij})$, where t is the temperature and e_{ij} – the deformation tensor, and
- thermal boundary conditions, valid for the deformed configuration, may be applied only provided that the displacements and strains are known.

Uncoupling of thermal and mechanical terms in eq. (1) is possible according to the following.

- In order to neglect dimensional changes due to transformation from an undeformed to a deformed configuration, it is necessary to assume that $dA/dA_0 = 1$ and $dV/dV_0 = 1$, so that $dh = dh_0$ and $d\rho_0 = d\rho$, *i. e.* ρ is temperature independent. Typical density values at both room and liquidus temperatures for PbSb alloys that are applied in welding differ up to 6%. This error has little effect on the numerical analysis and determination of residual stresses, since they appear at relatively low temperatures. The error is to be accounted for when analysing the temperature or heat distribution.

- Deformation dependence of strain energy density rate opposed to the temperature dependence may be omitted according to the following expression:

$$\dot{u} = \frac{\partial u}{\partial T} \dot{T} + \frac{\partial u}{\partial e_{ij}} \dot{e}_{ij} \quad (2)$$

The first term is proportional to mass density r and heat capacity c , and the second term to yield strength $R_{p0.2}$ and the thermal coefficient α . The change in both thermal and mechanical energy for the PbSb alloy is given in tab. 1. Apparently, the error becomes less than 1% when comparing the change in thermal and mechanical energy, as $\Delta u_t = \rho c \Delta t$ [Jcm^{-3}] ($\Delta t = 1$ K) and $\Delta u_m = 3\alpha R_{p0.2}$. The comparison is made at room temperature, since the change in mechanical energy is even smaller at higher temperatures (R_p decreases considerably).

Table 1. Energy comparison for the PbSb alloy

Density, ρ [gcm^{-3}]	Heat capacity, c [$\text{Jg}^{-1}\text{K}^{-1}$]	$\Delta u_t = \rho c$ [Jcm^{-3}]	Coefficient of thermal expansion, α [K^{-1}]	Yield stress, $R_{p0.2}$ [Nmm^{-2}]	$\Delta u_m = 3\alpha R_{p0.2}$ [Jcm^{-3}]
11	0	1	$2.76 \cdot 10^{-3}$	7	0

- By using similar arguments, the pure mechanical energy term $\int_{V_0} T^{ij} v^i dV_0$ in eq. (1) can also be omitted.

These approximations allow for eq. (1) to be written in the uncoupled form as:

$$\int_{V_0} \rho_0 (r + \dot{u}) dV = \int_{A_0} h_0 dA_0 \quad (3)$$

By applying the Gauss' theorem, eq. (3) is transformed to eq. (4), and taking into account that at the boundary surface A_0 , the relation for the introduced heat conduction vector, q^i , defined by heat flux h and external unit normal n_i , is given by $q^i n^i = h_0$, and for Descartes co-ordinates, x^i :

$$\int_{V_0} \rho_0 (r + \dot{u}) dV - \int_{A_0} q^i n^i dA_0 = 0 \quad (4)$$

If $\rho_0 r$ is replaced by Q_v , and $\rho_0 \dot{u}$ is replaced as $\rho_0 (\partial u / \partial T) \dot{T} = \rho_0 c \dot{T}$, where c is specific heat capacity, and we shall also omit index "0", thus ignoring the difference between the current and reference configuration, eq. (4) becomes:

$$\int_{V_0} (Q_v - \rho c \dot{T}) dV - \int_{A_0} q^i n^i dA_0 = 0 \quad (5)$$

To solve this equation we introduce the constitutive material law, i. e. the Fourier law of heat conduction:

$$q^i = -k^{ij} \frac{\partial T}{\partial x^j} \quad (6)$$

where k_{ij} is the tensor coefficient of thermal conductivity. Finally, the heat transfer equation is:

$$\int_{V_0} \left(\frac{\partial}{\partial x^i} k^{ij} \frac{\partial T}{\partial x^j} + Q_v - \rho c \dot{T} \right) dV = 0 \quad (7)$$

Besides being non-stationary, eq. (7) is non-linear because of the temperature dependence of material properties. The initial condition is given as $T(x^i, 0) = T_0(x^i)$, and the boundary conditions for temperature, heat flux, heat convection (fig. 1) are:

$$\begin{aligned} T &= T_s(x^i) && \text{(on } S_1) \\ q^i n^i &= q_s && \text{(on } S_2) \\ q^i n^i &= h(T_s - T_\infty) && \text{(on } S_3) \end{aligned} \quad (8)$$

where T_s and T_∞ are the given source and environmental temperatures, in respect; h is the convection heat-transfer coefficient, and q_s – the given heat flux.

Such a problem cannot be solved analytically in general, and requires numerical methods. This becomes more complicated when considering specific problems regarding the welding process, such as phase and structural change, welding heat input, weldment crystallisation, and location of liquidus and solidus surfaces. Equation (7) will be solved by applying the Galerkin method. The whole procedure is described in ref. [10].

Volume V is divided into E finite elements, each having p nodes. Assume the change in T for each element e as:

$$T^e(x^i, t) = N^k(x^i) T_k(t) \quad (9)$$

where $T^e(x^i, t)$ is the temperature distribution inside element e , $N_k(x^i)$ – the interpolation function, and T_k – the nodal temperature. The partial differentials are:

$$\frac{\partial T^e}{\partial x^i} = \frac{\partial N^k}{\partial x^i} T_k = N_i^k \dot{T}_k, \quad \frac{\partial T^e}{\partial t} = N^k \dot{T}_k \quad (10)$$

where N^k is the matrix of the order $n \times r$ (n – space dimension, r – number of elements). By multiplying eq. (7) by weight function chosen to be identical to N^k , and integrating over each finite element, $i. e.$ by applying the Galerkin procedure, we obtain:

$$\int_{V^e} \frac{\partial}{\partial x^i} k \frac{\partial T}{\partial x^i} N^k dV - \int_{V^e} \rho c \dot{T} N^k dV = 0 \quad (i = 1, 2, \dots, p) \quad (11)$$

By applying the Gauss' theorem, the first term may be written as:

$$\int_{V^e} \frac{\partial}{\partial x^i} k \frac{\partial T}{\partial x^i} N^k dV = \int_{V^e} k \frac{\partial T}{\partial x^i} N_i^k dV - \int_{S^e} k \frac{\partial T}{\partial x^i} n^i N^k dS \quad (12)$$

The surface integral over S^e is divided into S_1^e , S_2^e , and S_3^e , according to boundary conditions (fig. 1). The surface integral in eq. (12) over S_1^e equals 0. Boundary conditions over surfaces S_2^e and S_3^e are given in eq. (8), and the surface integral in eq. (12) satisfies these boundary conditions, so we write:

$$\int_{S_2^e} k \frac{\partial T}{\partial x^i} n^i N^k dS - \int_{S_2^e} q_s N^k dS_2 - \int_{S_3^e} h(T_s - T_\infty) N^k dS_3 \quad (13)$$

The discretized heat conduction equation is further written in matrix form:

$$C^{kj} \dot{T}_j - (K_c^{kj} + K_h^{kj}) T_j - R^k = 0 \quad (14)$$

$$R^k = R_Q^k + R_q^k + R_h^k \quad (15)$$

where C^{kj} is the heat capacity matrix, K_c^{kj} and K_h^{kj} are the matrices of heat conduction and convection transfer, in respect, and R^k, R_Q^k, R_q^k , and R_h^k are vectors of the heat load, due to volume heat source, heat flux, and convection, respectively. Equation (14) can be solved by explicit or implicit procedure [11], so we can determine temperature values among nodes, or the temperature distribution.

Phase change is a characteristic of the welding process accompanied by the release of latent heat. This process demands for specific modifications to the numerical procedure for solving the heat conduction equation. This is usually simulated by an additional heat source in a part of the domain between solid and liquid, and solution accuracy is strongly affected by the location of these domains. However, it is more suitable to simulate latent heat release by applying one of three alternative methods shown here.

The first method assumes latent heat as a part of heat capacity [1], simulating its release as a discontinuity of ρc . Thus, latent heat release is uniform. This method requires a fine mesh of finite elements and short time-steps.

The second method uses enthalpy to describe latent heat, accordingly $\rho c = dh'/dt$, where h' is specific enthalpy – a continuous function of temperature as opposed to heat capacity. The enthalpy relation is simply applied by replacing the differential with finite quantities, as $\rho c = \Delta h'/\Delta t$.

In the third method, the release of latent heat is assumed from a fictitious heat source volume of certain nodes of the finite element mesh [12]. Intensity of this source is equal to the release rate of the phase-change energy.

Theoretical analysis of residual stresses

Residual stresses are defined here as thermal stresses caused by non-uniform heating and cooling of the welded joint [9]. More detailed explanation is given in fig. 2, where the spatial and time distribution of temperature and stress (in the transverse direction) are illustrated for four characteristic stages of the resistance welding cycle (A, B, C, and D). The first stage (A) involves the positioning of the two parts for welding, and no thermal stresses are generated since there is no influence of heat. In the second stage (B), the electrodes are brought to the surface of the metal sheets and a slight amount of

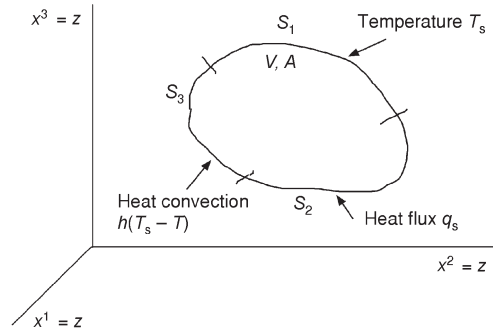


Figure 1. Domain and boundary conditions

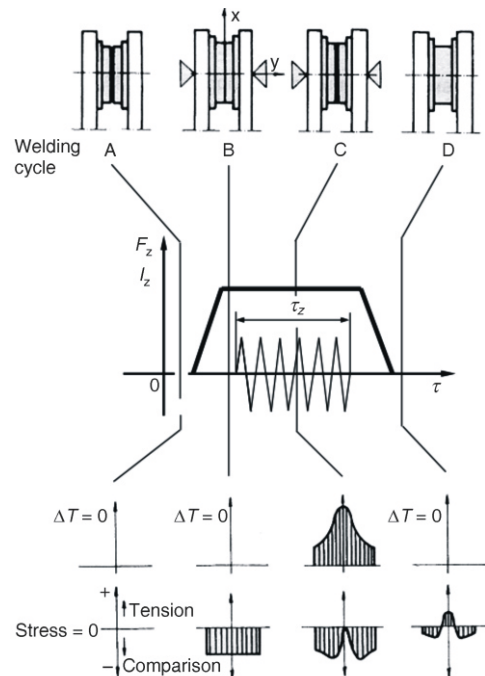


Figure 2. Distribution of temperature and residual stresses in the welding cycle

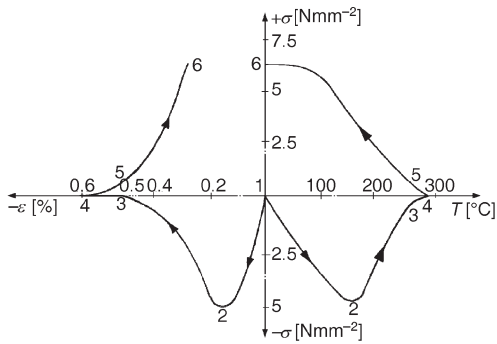


Figure 3. Stress-strain and stress-temperature dependence at welded joint centre [13]

pressure is applied, causing compressive stresses in metal sheets. These stresses are proportional to the force applied for welding. In the third stage (C), the current from the electrodes is applied briefly and the temperature increases to melting point at contact locations. Due to the high increase of temperature in this stage, the compressive stress increases as a result of thermal expansion of the material. In the liquid zone of the material, stresses are practically zero since there is no resistance to thermal forces. In the fourth stage (D) the welding current is removed and the acting force stops. The material cools and tends to shrink in the central cross-section. This is suppressed by the surrounding material with much lower temperature gradients. So the situation is opposite in behaviour to that in stage B. Thus, tensile stresses may arise that are balanced by remote compressive

pressure is applied, causing compressive stresses in metal sheets. These stresses are proportional to the force applied for welding. In the third stage (C), the current from the electrodes is applied briefly and the temperature increases to melting point at contact locations. Due to the high increase of temperature in this stage, the compressive stress increases as a result of thermal expansion of the material. In the liquid zone of the material, stresses are practically zero since there is no resistance to thermal forces. In the fourth stage (D) the welding current is removed and the acting force stops. The material cools and tends to shrink in the central cross-section. This is suppressed by the surrounding material with much lower temperature gradients. So the situation is opposite in behaviour to that in stage B. Thus, tensile stresses may arise that are balanced by remote compressive

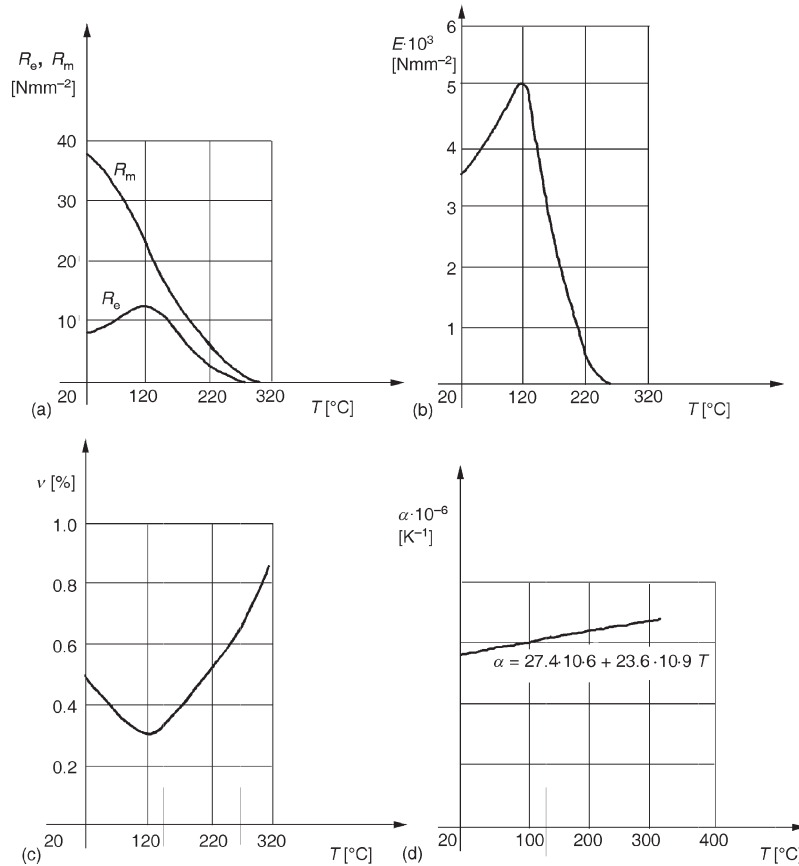


Figure 4. Temperature dependence of material characteristics for the PbSb 2 alloy

stresses. When the parts have cooled completely, with no temperature gradients in the welded zone, material behaviour is basically the same as in stage D, but with much higher tensile stresses, since the material's resistance to thermal forces is much higher at lower temperature.

Based on the explanation of the appearance of residual stresses in resistance welding, disregarding the presence of working stresses during the welding process itself, the temperature dependence of material properties is obvious. This fact is even more pronounced when stress vs. temperature and stress vs. strain are analysed at the centre of weldment cross-section, fig. 3, and disregarding working stress.

The welding cycle is denoted by points 1-4 on both diagrams (fig. 3), and the cooling cycle by points 4-6. The decrease in modulus of elasticity with rising temperature explains the non-linearity of the stress-strain curve between points 1 and 2. Point 2 corresponds to yield stress, followed by a decline in stress, because the yield stress is reduced by further heating of the material up to point 3 when it reaches zero. Stresses have diminished up to point 4, but significant plastic strain gradually arises. The elastic strain recovers during the cooling cycle, and tensile stress appears and grows non-linear due to the rise in the elasticity modulus as the temperature lowers (4-6). Point 6 denotes the end of the welding process with residual stresses and strains.

In fig. 4, the temperature dependences of PbSb 2 alloy properties are illustrated (yield stress and tensile strength, fig. 4(a), modulus of elasticity, fig. 4(b), Poisson's ratio, fig. 4(c), and the linear thermal expansion coefficient, fig. 4(d). As already stated, yield stress and elasticity modulus decrease with temperature, so that yield stress is practically zero at 250 °C, while at 700 °C material stiffness diminishes (modulus of elasticity equals 0). Other PbSb alloys for resistance welding (from PbSb 1 to PbSb 4) have a similar behaviour.

Application of the finite element method to residual stresses

The basic procedure of the finite element method application to residual stress evaluation is essentially the same as for the heat conduction problem [9] and includes domain discretization (division into finite elements), interpolation of all quantities inside finite elements, integration over each element, and solving of the resulting equation system. The major differences are in the equations to be solved, because displacement is the independent variable in the residual stress problem instead of temperature, the static equilibrium equations are solved instead of heat conduction equations, and material behaviour is described by the stress-strain relation instead of the Fourier law. So, it is necessary to introduce isoparametric interpolation functions for displacements as follows:

$$u^i(x^j, t) = N^K(x^j)u_k^i(t) \quad (16)$$

where $u^i(x^j, t)$ is the displacement distribution inside an element, t – the time, $N^K(x^j)$ – the interpolation function, $u_k^i(t)$ – the nodal displacement, and x^j – the Descartes co-ordinates. Now, we write:

$$e_{k\ell} = \frac{\partial u^k}{\partial x^\ell} = \frac{\partial N^k}{\partial x^\ell} u_k^k = N_\ell^k u_k^k \quad (17)$$

where N_ℓ^k is the matrix of the order $n \times r$ (n – space dimension, r – number of element nodes). Geometrical non-linearity is neglected as a justified assumption for the problem considered. On the other hand, material non-linearity cannot be neglected, leading to the expression for total incremental strain comprising the elastic, plastic, and thermal components.

$$d\varepsilon_{k\ell} = d\varepsilon_{k\ell}^e + d\varepsilon_{k\ell}^{ep} + \delta_{k\ell} d\varepsilon^T \quad (18)$$

The elastic strain is related to the stress by the following equation (Hooke's law):

$$d\sigma_{ij} = E_{ijkl} d\epsilon_{kl}^e \quad (19)$$

where $d\sigma_{ij}$ is the stress tensor increment, and E_{ijkl} – the elasticity tensor.

Plastic strain may be expressed by applying the theory of incremental plasticity, taking into account the normality condition, the von Mises yield criterion and the material strain strengthening assumption:

$$d\epsilon_{ij}^p = \frac{3}{2} \frac{d\epsilon_e^p}{\sigma_e} S_{ij} \quad (20)$$

where S_{ij} is the stress deviator tensor, and $d\epsilon_{ij}^p$ and σ_e are the equivalent plastic strain increment and stress, in respect, given by:

$$\sigma_e = \sqrt{\frac{3}{2} S_{ij} S_{ij}} \quad d\epsilon_e^p = \sqrt{\frac{3}{2} d\epsilon_{ij}^p d\epsilon_{ij}^p} \quad (21)$$

Thermal strain, $d\epsilon^T$, can be expressed as follows if the transformation plasticity is neglected:

$$d\epsilon^T = \alpha dT \quad (22)$$

where α is the coefficient of linear thermal expansion, and dT – the temperature change.

Solving matrix equations

An explicit procedure is applied for the numerical integration of differential equations based on initial temperature distribution, $T_0 = T(x^i, 0)$. If the time derivative of the temperature vector in eq. (14) is written as:

$$T = \frac{\Delta T}{\Delta t} \frac{T_{n+t} - T_n}{\Delta t} \quad (23)$$

where Δt is the time interval. Then eq. (14) may be written in explicit form:

$$\begin{aligned} C^{kj} (T_{n+t}^j - T_n^j) - (K_c^{kj} - K_h^{kj}) T_n^j \Delta t - R^k \Delta t \\ C^{kj} T_{n+t}^j - C^{kj} T_n^j - R^k \Delta t - (K_c^{kj} - K_h^{kj}) T_n^j \Delta t \end{aligned} \quad (24)$$

The explicit procedure saves much calculation time due to the direct linking of unknown variables in two successive steps, T_{n+t} and T_n . However, two requirements need to be fulfilled:

- $(K_c^{kj} - K_h^{kj})$ is a diagonal matrix [14], and
- procedure stability depends on the time-step that should be adopted to be extremely short [15].

Thermomechanical modelling applied for analysis of resistance spot welding of PbSb alloy

Problem definition

We shall define the mathematical modelling of resistance spot welding of PbSb alloys using the example of the welding process on stacked positive and negative battery plates (lead-acid battery cells) in the assembly of the polypropylene (PP) battery case, fig. 5.

Stack assembly is produced by an automatic machine, and welding is performed through PP case walls across the intercell connector. The welding machine is equipped with a

hydraulic unit that provides a constant welding force, and a power unit for the metal fusion process. It is possible, within limits, to vary pressure force, current, voltage, and time of the welding process.

The welding cycle is comprised of three stages (compressing, welding, and holding) and may last within 1 to 50 periods or, from 0.02 s to 1 s. The welding force can change from 0.5 kN to 1.5 kN. The basic resistance spot welding cycle of the PbSb alloy is shown in fig. 6.

The time and welding force may differ for various PbSb alloys. Battery cells are made of PbSb or PbCa alloys of various content, depending on the battery type. The chemical composition of a battery cell alloy directly affects the chemical composition of the intercell connector to be resistance spot welded and will serve as an illustration for the numerical simulation of the resistance spot welding of intercell connectors made of several PbSb alloys.

Material for battery intercell connectors

The material for battery intercell connectors is the PbSb alloy. The most common chemical composition is given in tab. 2. Other alloying elements that are given in tab. 2 have no considerable effect on thermal, mechanical and electrical properties of the alloy.

Physical model

The physical model is a designated intercell connector with all the necessary elements for the welding behaviour as a whole. Assuming that the behaviour of every intercell battery connector during welding is almost the same, the connector shown in fig. 7 is adopted as the problem domain. The resistance welding process is modelled as a heat transfer process with initial and boundary conditions.

The initial condition is given as a temperature distribution $T_0 = 20\text{ }^\circ\text{C}$ at $t = 0$ over the whole domain. Boundary conditions are defined

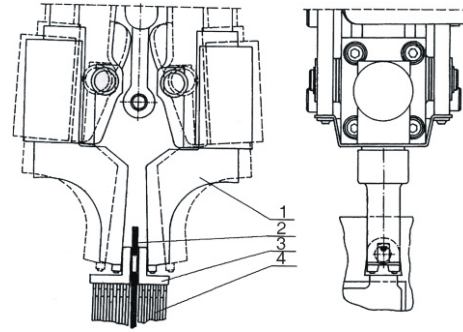


Figure 5. Resistance spot welding of battery cells
 (1) – welding machine; (2) – PP case, (3) – intercell connector, (4) – battery cell stack

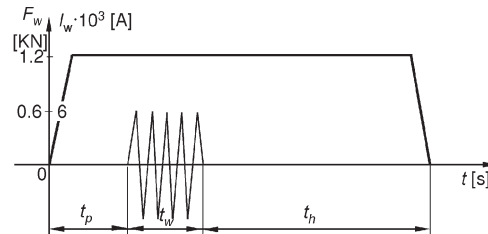


Figure 6. The resistance spot welding cycle
 t_p – compression time, t_w – welding time, t_h – holding time

Table 2. Chemical composition of the PbSb alloy

No.	Alloy (internal code)	Alloying elements			Pb
		Sb	Sn	Other	
1	SDS	3.28	0.43	0.17	96.12
2	SD	3.4	0.06	0.24	96.3
3	A4	2.67	0.12	0.26	96.95
4	DD	2	0.27	0.17	97.56

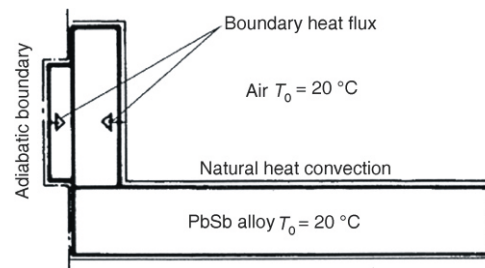


Figure 7. Initial and boundary conditions

for: the air boundary as heat convection from the PbSb alloy into air of temperature $t_{\infty} = 20$ °C; the electrode boundary as heat is conducted through the PbSb alloy during welding, and later as heat is also convected from the PbSb alloy into air; and the boundary where two elements come into contact and at the part of the wall case, acting as an adiabatic boundary. At the boundary of two elements, the heat load consists of heat flux of contact and ohmic resistances, and the heat load at electrode domain contact boundary – as heat flux of metal sheet electrode contact resistance. The equation and heat convection coefficient need to be defined for heat transfer by natural convection from PbSb alloy into surrounding air.

Heat is transferred from the case wall into surrounding air by free flow. In general, the free fluid flow equation (along and around geometrical shapes) applied for this special case is:

$$Nu = 1.18 GrPr \quad (25)$$

and it enables the determination of the convective heat transfer coefficient:

$$h = \frac{Nu\lambda}{L} \text{ [Wm}^{-2} \text{ C}^{-1}] \quad (26)$$

where L is the characteristics of geometry [m], and λ – the thermal conductivity of air [Wm⁻¹°C⁻¹].

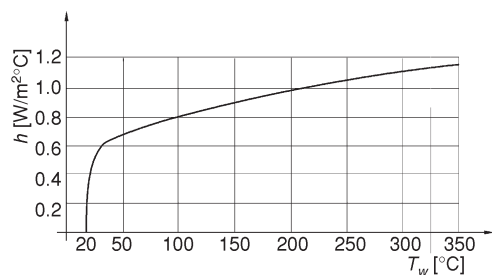


Figure 8. Case wall temperature dependence of the heat conductance coefficient

The change of the convective heat transfer coefficient depending on the battery case wall temperature is shown in fig. 8.

A particular problem represents the part of the analysed battery intercell case, which in fact is 3-D, and analysis of 3-D problems is very complicated and demands application of high capacity computers. Reducing 3-D to a 2-D problem is emphasized in this example having in mind the dilemma of representing the model as planar or axis-symmetrical. Namely, boundary conditions may be planar, while the body shape (the cylindrical part in particular) has axis symmetry. However, since the planar part could not be included within the same meridian section, thus the axis-symmetrical representation is disregarded. All in all, specific details of the resistance spot welding process must be incorporated into this physical model.

The resistance spot welding is usually characteristic in the appearance of molten weld splashes or bursts, because of the rapid heating in phase change temperature ranges. Multiple increase of heat capacity in relatively short temperature intervals (around 300 °C) apparently has a considerable effect on the rapid change of temperature, and may create high local stresses and cause splashes and bursts. Principally, a similar analysis might include the stress state in the welding zone by solving an appropriate elastic-viscous-plastic boundary problem.

Methodology of problem solving and resistance spot welding specifics

Solving the non-stationary non-linear equation is principally explained [10], where a detailed analysis recommends use of explicit time integration over short time-steps, and with a reduced specific heat matrix. Based on the known initial temperature distribution, a further inte-

gration over time is made according to the scheme given by eq. (24). The index “ n ” in eq. (24) corresponds to initial state, and index “ $n + t$ ” to the final state within the n^{th} time-step. The heat conductivity matrix $(K_c^{kj} \ K_h^{kj})$, the reduced specific heat matrix C^{kj} , and the heat load vector R^k , all change with each time-step depending on the previous temperature distribution. For a homogeneous isotropic material, an automatic alteration of all necessary matrices and vectors is made simple by embedding functional temperature dependences of corresponding material properties. The time-step needs to be sufficiently short in order to achieve stability of the explicit scheme. In this case, sufficiently short means:

$$\Delta t_{cr} \leq \frac{2}{\xi_{\max}} \quad (27)$$

where ξ_{\max} is the maximal value in the corresponding problem of eigenvalues [14]. The eigenvalue problem is not difficult to formulate and solve, but requires additional effort and calculation time, and additionally, ξ_{\max} also changes with each calculation step. Hence, the authors’ estimate is to decide upon Δt_{cr} value in advance and based on the analysis in tab. 3.

Table 3. Time-steps (no. of steps × time [s])

						Total			
Fine step	100	0.001	990	0.01	500	0.1	540	1	600 [s]
Coarse step	10	0.001	99	0.01	90	0.1	590	1	600 [s]

Most of the calculation time is spent for matrix multiplication, e. g. $(K_c^{kj} \ K_h^{kj})T_n^j$ in eq. (24) needs special attention so to avoid unnecessary multiplication with a majority of zero elements in $(K_c^{kj} \ K_h^{kj})$. A rough estimate for an approximately rectangular domain discretised with a 60×60 node mesh implicates there are about 98% zero elements in the heat conductivity matrix. In other words, only 1/60 locations are occupied in the matrix that are multiplied by T_n^j .

Solidus and liquidus positions are determined based on temperature distribution, and yet their locations also influence the temperature distribution. This conjugate system requires an extremely short time-step, independent of procedure stability, thus justifying that $\Delta t_{cr} = 0.001$ s as the welding interval [16]. It seems beneficiary to linearize the problem in this way than to apply complicated procedures for solving non-linear problems, i. e. Newton-Rason method. Temperature distribution in each time-step is given for nodes and it is quite difficult to determine liquidus and liquidus locations. liquidus and liquidus lines are required to pass through nodes in order to define a solid, liquid, or mixed state in each finite element. It is clear that this can be achieved only approximately, and that the number of nodes, or the finite element mesh, considerably affect accuracy. A triangular finite element mesh is used here and shown in fig. 9, with a constant temperature gradient inside the finite elements, and with pre-selected point locations (T1-T5).

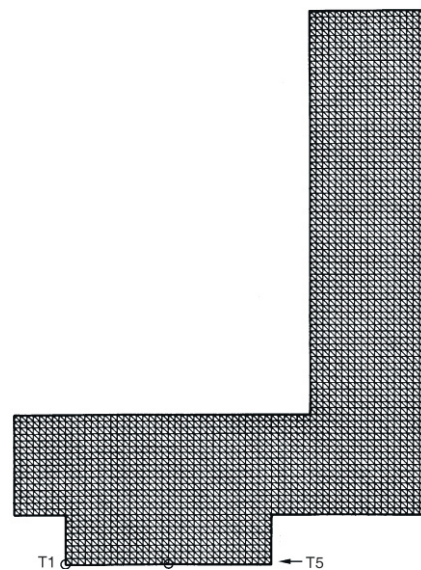


Figure 9. The finite element mesh – fine

Results for spatial and time distribution of temperature

Results of thermal calculation obtained according to the defined procedure are illustrated in figs. 10(a)-(d) showing isotherms at certain time intervals, and in fig. 11(a) and (b) showing diagrams of temperature-time dependence for two of the selected locations in fig. 9. All of these results are for alloy A4 (see tab. 2).

Adequate contact surface geometry (spherical shape) has accomplished the initial melting point to be reached at welding zone centre, and not at its perimeter (circumference) as it is achieved when classical resistance spot welding is performed [17].

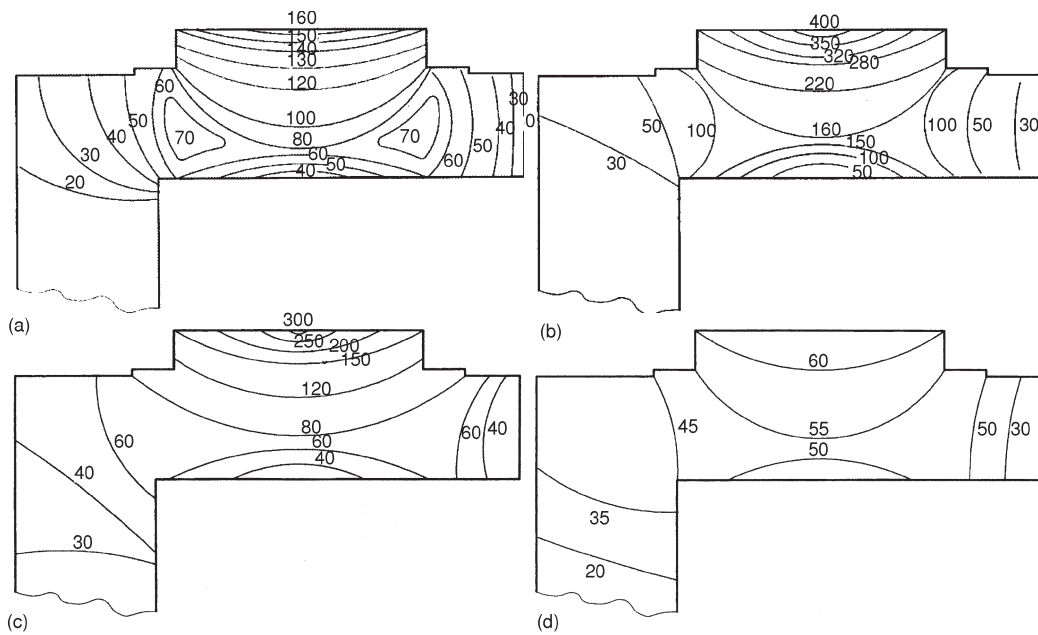


Figure 10. Spatial temperature distribution
 (a) $t = 0.001\text{ s}$, (b) $t = 0.1\text{ s}$, (c) $t = 1\text{ s}$, (d) $t = 60\text{ s}$

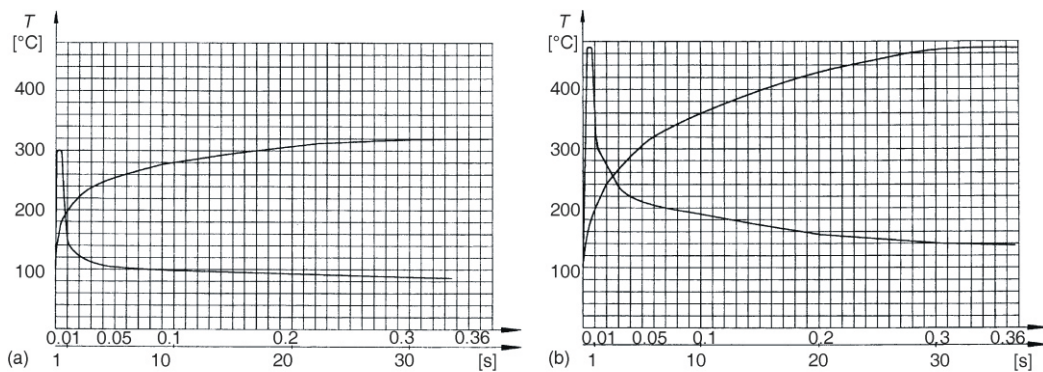


Figure 11. Temperature-time dependence at points T1 (a) and T5 (b)

Conclusions

The degree of knowledge and understanding of the complex phenomena in thermal, mechanical, and electrical processes that determine the welding process, as well as acquiring data on mechanical and metallurgical properties of the applied techniques conducted at high temperatures are the crucial factors in the process of creating and finalizing the mathematical model. Of particular importance is the necessity to accumulate and have quality data of physical and mechanical properties of metals at temperatures close to melting, or more precise, at temperature intervals within the liquidus and liquidus lines.

The applied mathematical method enabled efficient and qualitative analysis regarding: temperature field determination and its influence on the welding process, (eq. 24), and application of real intermediate conditions (particularly boundary conditions) in the initial stage of the mathematical analysis, whereas possibilities for errors are reduced during the creation of the analytical model.

The model for resistance spot welding of PbSb alloys is developed with respect to the real geometry of the welding zone, and physical and metallurgical properties of PbSb alloys and electrode material. The model takes into account phase transformation in the region of liquidus and liquidus temperatures, or latent heat transformation. Contact resistances on contact surface zones: electrode-metal sheet, and sheet-sheet are analytically involved, while the influence of the actual welding force has proved to be negligible.

References

- [1] Crivelli, L. A., Idelshon, S. R., A Temperature-Based Finite Element Solution for Phase-Change Problems, *International Journal for Numerical Method in Engineering*, 23 (1986), 1, pp. 99-119
- [2] Lazaridis, A., A Numerical Solution of the Multidimensional Solidification (or Melting) Problem, *International Journal Mass Transfer*, 13 (1970), 9, pp. 1459-1477
- [3] Sikarskil, D. I., Bolly, B. A., The Solution of a Class of Two-Dimensional Melting and Solidification Problem, *International Journal Solid Structure*, 1 (1965), 2, pp. 207-234
- [4] Orlov, D., Technology and Equipment of Contact Welding (in Russian), Mashinostroenie, Moscow, 1975, and 1986
- [5] Nakata, S., et al., In-Process Quality Control of Spot Weld by Detecting Voltage between Electrode Tips – Adaptive Control for Quality Assurance of Resistance Spot Weld in Real Time (2nd report), IIW Doc. III-719-82, 1982
- [6] Nied, H. A., The Finite Element Modeling of the Resistance Spot Welding Process, *Welding Journal*, 63 (1984), 4, pp. 123s-132s
- [7] Rice, W., Funk, E. J., An Analytical Investigation of the Temperature Distributions during Resistance Welding, *Welding Journal*, 46 (1967), 4, pp. 175s-186s
- [8] Sedmak, A., Numerical Simulation of the Welding Process – I part: Temperature fields (in Serbian), *Zavarivanje i zavarene konstrukcije*, 41 (1996), 1, pp. 5-12
- [9] Sedmak, A., Numerical Simulation of the Welding Process – II part: Residual stresses (in Serbian), *Zavarivanje i zavarene konstrukcije*, 41 (1996), 2, pp. 131-137
- [10] Kalaba, D., Thermomechanical Modelling of the Resistance Welding Process of PbSb Alloy (in Serbian), Ph. D. thesis, University of Priština, Faculty of Mechanical Engineering, Priština, Serbia, 1998
- [11] Berković, M., Maksimović, S., Sedmak, A., Analysis of Welded Joints by Application of the Finite Element Method (in Serbian), in: IFMASS 3 “Fracture Mechanics of Welded Joints” (Ed. S. Sedmak), Lectures presented at the Third International Fracture Mechanics Summer School, Arandjelovac, Serbia, 1984, GOŠA Institute and Faculty of Technology and Metallurgy, University of Belgrade, pp. 111-128

- [12] Bon, E., Nigro, L., Sanpietri, C., Numerical Solution of Thermal Processes with State and Phase-Change: The Computer Code Aten-2D, *Proceedings, ICNMNL Problems*, Dubrovnik, Yugoslavia, 1986, pp. 951-963
- [13] Easterling, K., Introduction to the Physical Metallurgy of Welding, Butterworths Co., London, 1982
- [14] Huebner, K. H., Thornton, E. A., Finite Element Method for Engineers, 2nd ed. John Wiley & Sons, New York, USA, 1982
- [15] Sahm, P., Numerical Simulation and Modelling of Casting and Solidification Processes for Foundry and Cast-House, CIATF, Zürich, Switzerland, 1984
- [16] Bathe, K. J., ADINAT-A Finite Element Program for Automatic Dynamic Incremental Nonlinear Analysis of Temperatures, AVL Report 82442-5, Mechanical Engineering Department, M.I.T., 1977
- [17] Bentley, K. P., Greenwood, J. A., Knowlson, P. M., Backer, R. G., Temperature Distribution in Spot Welds, *British Welding Journal*, 10 (1963), 12, pp. 613-619